Effect of surface stoichiometry on the band gap of the pyrite $FeS_2(100)$ surface

Y. N. Zhang,[1] J. Hu,[1] M. Law,[2] and R. Q. Wu[1,*]

[1]*Department of Physics and Astronomy, University of California, Irvine, California 92697, USA*

[2]*Department of Chemistry, University of California, Irvine, California 92697, USA*

(Received 15 February 2012; published 28 February 2012)

Systematic spin-polarized density functional calculations were performed for a series of pyrite $FeS_2(100)$ surfaces to clarify the effect of surface stoichiometry on stability, electronic structure, and band gap. While the bulk FeS_2 is nonmagnetic, the topmost layer of the stoichiometric and S-deficient $FeS_2(100)$ surfaces are spin polarized, with magnetic moments of 2 μ_B or 4 μ_B per Fe. These surfaces also have sizeable band gaps, 0.56–0.72 eV; they hence can be useful for spintronic and photovoltaic applications. On the contrary, S-rich surfaces have small-gaps, <0.3 eV, which might be responsible to the low open-circuit voltage of pyrite solar cells.

DOI: 10.1103/PhysRevB.85.085314 PACS number(s): 72.40.+w, 71.20.Nr, 73.20.−r, 75.50.Pp

I. INTRODUCTION

Iron pyrite (FeS_2) is experiencing a resurgence of interest for use in solar photovoltaic and photoelectrochemical cells due to its suitable band gap (0.9–0.95 eV), excellent optical absorptivity, and essentially infinite abundance of iron and sulfur in the planet's crust.[1] The main hurdle to the use of pyrite continues to be the low open-circuit voltage (V_{OC}) of pyrite devices (<200 meV or ∼20% of the band gap),[2,3] which may result from gap states created by surface and bulk defects.[4,5] Although the first pyrite solar cells were reported in the 1980s, there is still no clear strategy for improving the solar energy conversion efficiency of this material. To make major breakthroughs, new fundamental research on pyrite aims to understand the interplay between stoichiometry, structure, and electronic properties of pyrite thin films and their surfaces.

The pyrite(100) surface is typically nonstoichiometric and often features a complex nanoscale morphology and surface chemistry.[6] Cleavage of only Fe-S bonds perpendicular to a (100) plane creates the stoichiometric (100) surface, which has an electronically stable cation (Fe^{2+}) and anion (S_2^{2-}) configuration. However, cleavage of S-S bonds—which is common on real pyrite surfaces—creates sulfur monomers (S^{1-}), which may convert to the more stable monosulfide (S^{2-}) through the redox reactions $Fe^{2+} + S^{1-} \rightarrow Fe^{3+} + S^{2-}$ or $2S^{1-} \rightarrow S^0 + S^{2-}$. Theoretical calculations using density functional theory (DFT), Hartree-Fock, and molecular dynamics methods have reported inconclusive and sometimes conflicting results on the surface band gap in particular, even for the stoichiometric $FeS_2(100)$ surface.[7–11] More systematic studies are needed to clarify key issues, including the following. (i) What are the stable configurations of pyrite(100) under different growth and annealing conditions? (ii) What is the impact of surface stoichiometry and morphology on the band gap of pyrite? (iii) Are intrinsic surface states and/or surface sulfur nonstoichiometry responsible for the low photovoltage of pyrite solar cells? Answers to these questions are also indispensible for the development of other promising photovoltaic technologies, such as CIGS and CZTS, to name a few. Moreover, the magnetization of Fe can be easily restored by removing its sulfur neighbors, as around vacancies in the bulk and also as near the surface and interface regions of pyrite.[12,13] Since pyrite has no precipitation problem, as inherent in most dilute magnetic semiconductors that use 3d magnetic dopants as sources of spin polarization, its unusual magnetic properties are very promising for spintronics applications.[14] This inspires us to conduct extensive DFT studies of crucial factors that govern the electronic properties of pyrite(100) surfaces.

II. METHODOLOGY AND STRUCTURAL MODELS

Theoretical calculations were performed using the Vienna Ab initio Simulation Package (VASP)[15] along with the projector augmented wave (PAW) method.[16] We used the generalized-gradient approximation (GGA)[17] to describe the exchange-correlation interaction among electrons. An energy cutoff of 350 eV was used for the plane-wave basis expansion. The DFT+U scheme[18] proposed by Dudarev *et al.*[19] was adopted for the treatment of Fe 3d orbitals, with parameters U equal to 2 eV, which give a lattice constant of 5.422 Å and an indirect band gap of 1.02 eV for the bulk pyrite, both in good agreement with the most widely accepted experimental values, 5.419 Å and 0.95 eV, respectively.[12,20,21] We noted that the band gap of bulk pyrite is only 0.50 eV without the U correction, and it increases to an unphysical 2.66 eV when hybrid functionals are used.[22] Thus, we believe that the approach and parameters presented here are well suited to the description of pyrite.

To simulate various $FeS_2(100)$ surfaces, we used a periodic slab model with eleven FeS_2 atomic layers per slab separated by vacuum layers ∼17 Å thick. A (2 × 2) supercell in the lateral plane was adopted to allow a sufficient degree of surface reconstruction and non-integer composition ratios. The stoichiometric (2 × 2) cell has 8 Fe + 16 S atoms per surface and 88 Fe + 176 S atoms per slab. As depicted in Fig. 1, we modeled nine $FeS_2(100)$ surfaces of different stoichiometry in order to establish a trend between surface composition and electronic structure. For convenience we denote the surfaces by Surf(n), where n is the deviation of surface composition ratio of sulfur and iron atoms relative to the stoichiometric $FeS_2(100)$ surface, which itself is denoted as Surf(0). The slabs were constructed with identical surfaces in order to avoid artificial electric fields in the vacuum for studies of polar surfaces. The lattice constant in the lateral plane was set according to the optimized lattice constant of bulk pyrite, a = 5.422 Å. The Fe and S atoms in the central layer were fixed at their bulk positions during the structural optimization procedure,

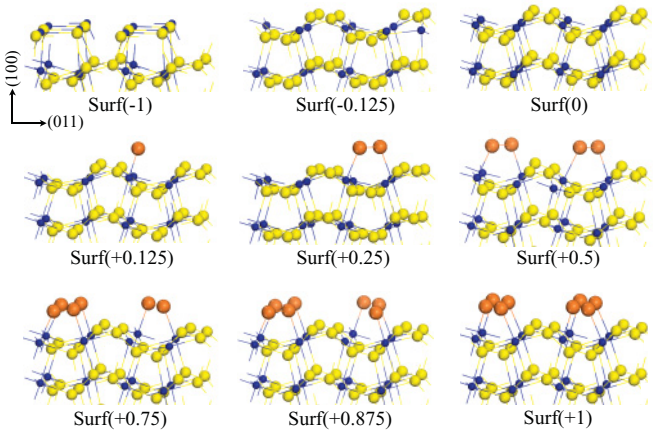

FIG. 1. (Color online) Relaxed structures of the nine $FeS_2(100)$ surfaces explored in this study. The yellow (light gray) and blue (medium gray) spheres represent S and Fe atoms, respectively. The large orange (dark gray) spheres represent the additional sulfur atoms added to the stoichiometric surface, Surf(0).

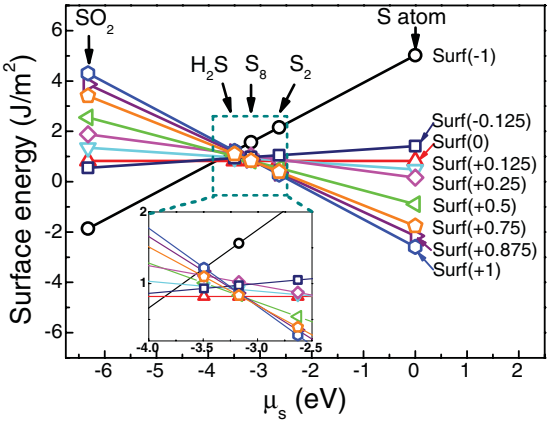

FIG. 2. (Color online) Calculated surface energies of different $FeS_2(100)$ surfaces versus the sulfur chemical potential, μ_S. The inset shows results in growth and annealing environments employing H_2S, S_8, or S_2 as the sulfur reservoir.

whereas all other atoms were fully relaxed until forces became smaller than 0.01 eV/Å.

III. RESULTS AND DISCUSSIONS

As a result of structural optimization, we observe that (i) Surf(0) shows no significant surface reconstruction, in agreement with previous reports[8]; (ii) Surf(−1) reconstructs, and the surface S and Fe atoms become nearly coplanar; and (iii) sulfur atoms added to Surf(0) form dimers for $n \geqslant +0.25$ with large energy gains of up to 0.4 eV/atom. To quantify the structural stability, we define the surface energy γ at temperature T and pressure p as

$$\gamma(T,p) = \frac{1}{2A}[G(T,p,N_{\mathrm{Fe}},N_S) - N_{\mathrm{Fe}}\mu_{\mathrm{Fe}}(T,p) - N_S\mu_S(T,p)]. \quad (1)$$

Here, A is the surface area, G(T, p, N_{Fe}, N_S) is the Gibbs free energy of the slab, and N_{Fe} and N_S are the numbers of Fe and S atoms. The chemical potentials of Fe (μ_{Fe}) and S (μ_S) obey the constraint $\mu_{Fe} + 2\,\mu_S = \mu_{FeS2}$, where μ_{FeS2} is the chemical potential of one FeS_2 formula unit in bulk pyrite. Under ambient conditions, G can be approximately replaced by the total energies from DFT calculations, without contributions from configurational or vibrational entropy.[23] Values of γ(T, p) are shown in Fig. 2 for μ_S ranging from the energy of a sulfur atom in SO_2 (−6.32 eV) to that of an isolated sulfur atom (0 eV) to simulate environments from oxidizing conditions to S-rich conditions.

The calculated surface energy of Surf(0) is 0.81 J/m^2, which falls in the range of 0.54–0.82 J/m^2 proposed by Ellmer and Hopfner based on experimental values of the compressibility and bulk moduli of $FeS_2(100)$.[24] Calculations without the U term lead to a larger γ(T, p) of 1.04–1.23 J/m^2 for Surf(0),[25,26] which again illustrates the importance of the Hubbard U correlation for the Fe-d orbitals in pyrite. From the data in Fig. 2 one finds that the equilibrium surface stoichiometry of $FeS_2(100)$ can be tuned by changing μ_S through the use of different pyrite growth and annealing environments. Interestingly, Surf(0) is stable only in a narrow window, -3.85 eV $< \mu_S < -3.17$ eV, and becomes less stable than either Surf(−1) under oxidizing conditions or Surf(+1) under S-rich conditions. Annealing in H_2S should favor Surf(0), while Surf(+1) is more stable when using S_8 or S_2 as the sulfur reservoirs.[27]

Now we discuss the effect of composition on the surface band gap. As a benchmark, we begin with Surf(0), which has been extensively explored in previous theoretical studies.[25,26] Using a simple ligand field model, Bronold *et al.* posited the existence of intrinsic Fe d_z^2 and d_{xy} surface states in the band gap (so-called a_1 and b_2 states) and used them to explain the low V_{OC} of pyrite cells.[6,28] However, recent DFT calculations by Sun *et al.*[25] found no surface states within the gap using either the GGA or GGA+U methods. This discrepancy is unsurprising since several features were missing in the Bronold model, including structural relaxation and charge transfer at the surface. We reproduced results of Sun *et al.* using a low-spin state for Surf(0), which is appropriate for bulk pyrite. However, our spin-polarized DFT+U calculations indicate that Surf(0) is actually magnetic with a moment of 2.0 μ_B per surface Fe atom (Fe_1). This high-spin state has a substantial energy gain, 1.87 eV/cell for $U = 2.0$ eV, compared to the low-spin state. Extensive testing indicates that the surface spin polarization is very stable for $U > 0.25$ eV in VASP calculations; it is already magnetic with a moment of 2.0 μ_B per surface Fe atom even for $U = 0$ eV through all-electron calculations using the full potential linearized segmented plane wave (FLAPW) method. Therefore, the ground state of Surf(0) and also other S-deficient surfaces are stably magnetic simply because some S neighbors of the surface Fe atoms are removed. After our submission Burton and Tsymbal also reported a conducting ferromagnetic interface between $LaAlO_3$ and FeS_2, and they assigned charge transfer from $LaAlO_3$ to a localized interface state of pyrite as the mechanism for spin polarization.[13]

As shown in Fig. 3(a), the high-spin Surf(0) has spin-dependent bands, with sizeable *direct* band gaps of 0.72 eV and 0.87 eV for the majority and minority spin channels, respectively. The two pronounced surface states in the majority spin channel: SS1 within the conduction band (CB) around

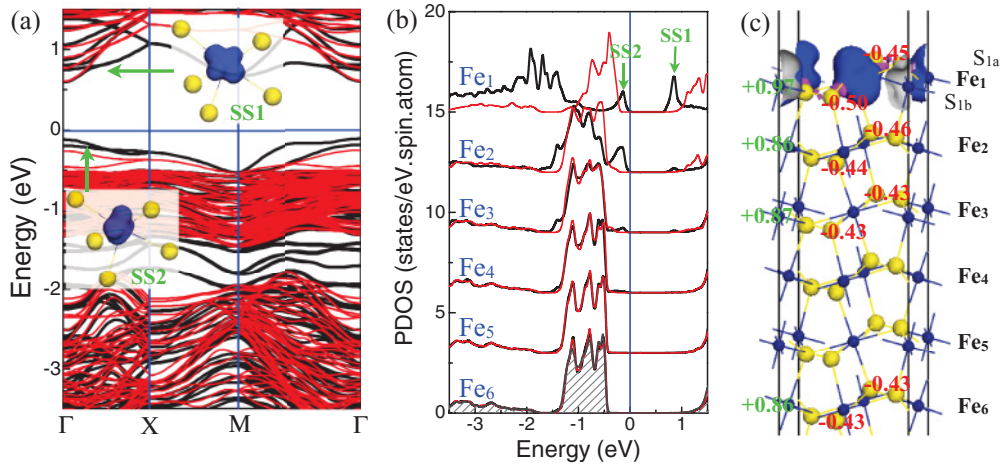

FIG. 3. (Color online) (a) The band structure of Surf(0). (b) The projected density of states (PDOS) for Fe atoms in different surface layers, labeled Fe_1 to Fe_6. In both (a) and (b), bold black and thin red (gray) lines denote states in the majority and minority spin channels, respectively; arrows highlight the two surface states (denoted SS1 and SS2) that determine the surface band gap (0.72 eV); zero energy gives the position of the Fermi level. Insets in (a) show the wave function features of SS1 and SS2; shaded region under the DOS curve of Fe_6 in (b) shows DOS of Fe in the bulk pyrite. (c) Isosurfaces of spin density and Bader charges of Surf(0). Positive and negative values of Bader charges represent electron depletion and accumulation on individual atoms. The atomic layers of Fe are labeled Fe_1 to Fe_6. S_{1a} and S_{1b} denote the sulfur atom layers above and below the first Fe layer. In (c) and insets of (a), yellow (light gray) and blue spheres represent sulfur and iron atoms, respectively.

the Γ-point and SS2 within the valence band (VB) at the M point but 0.37 eV above the VB at the Γ-point. From their wave-function features in the insets in Fig. 3(a), both SS1 (Fe-$d_{x^2-y^2}$-like) and SS2 (Fe-d_{z^2}-like) have the e_g characters and should originate from CB of pyrite. The projected density of states (PDOS) of Fe atoms in different surface layers are plotted in Fig. 3(b) to provide a depth-resolved picture of the Surf(0) electronic structure. It is obvious that the surface effect is limited to the top three atomic layers (∼7 Å total thickness). The unoccupied SS1 nearly vanishes by the second Fe layer (Fe_2), while the occupied SS2 somewhat extends into Fe_3. There is a marked splitting of the Fe_1 VB between the two spin channels, with the majority spin channel shifting ∼1 eV deeper in energy. Meanwhile, one surface t_{2g} band in the minority spin channel shifts into the CB due to the surface spin polarization. The electronic structure of Fe_4 and deeper layers resembles bulk pyrite as manifested by the close overlap between DOS curves of Fe_6 and that of Fe in the bulk pyrite, shown as the shaded region. Interior layers are nonmagnetic, and Fe t_{2g} and e_g states form the edges of the VB and CB, respectively. It is more evident from Fig. 3(c) that the spin polarization is mainly around Fe_1, while the contributions of Fe_2 and Fe_3 layers to the magnetic moment decrease rapidly to ∼0.03 μ_B and 0.00 μ_B, respectively. Our results suggest that Surf(0) may provide an ideal two-dimensional semiconducting spin-1 system for fundamental studies and spintronics applications.

We also calculated the net charge on each atom of the fully relaxed Surf(0) using the Bader charge-division scheme [Fig. 3(c)].[29] Relative to the charges of bulklike Fe (+0.86 electrons) and S (−0.43 electrons), each Fe_1 atom additionally loses 0.1 electrons (slight oxidation toward Fe^{3+}), while S_{1a} and S_{1b} atoms gain 0.02 and 0.07 extra electrons from their neighbors. Overall, Surf(0) is auto-compensated and charge neutral.

According to Fig. 2, two other important FeS_2(100) surfaces are Surf(−1), which has the lowest surface energy in oxidizing conditions, and the fully dimerized Surf(+1), which is more stable in S-rich conditions. Band structure calculations show that Surf(−1) and Surf(+1) have indirect band gaps of 0.71 eV and 0.3 eV, respectively [Figs. 4(a) and 4(b)]. As for Surf(0), the effects of surface termination are limited within a short range (∼7 Å). To establish a general trend, we present the surface band gap as a function of sulfur stoichiometry in Fig. 4. It is important that Surf(n) with $n \leqslant 0.125$ retain fairly large band gaps (>0.55 eV), while the band gaps of sulfur-rich surfaces ($n > 0.125$) average only 0.25 eV. Moreover, we found that most sulfur-rich surfaces become metallic if the dimerization of surface sulfur atoms is prohibited in the calculations, as marked by the blue triangle in Fig. 4(c). Since Surf(+1) is more stable than Surf(0) and Surf(−1) across a broad range of μ_S, our findings may explain the low V_{OC} of pyrite devices fabricated in S-rich conditions. These results also suggest that pyrite should be prepared with stoichiometric or sulfur-deficient surfaces for photovoltaic applications.

It is interesting to ask why the extremely sulfur-deficient Surf(−1) has a relatively large band gap. This surface is ferromagnetic with a large magnetic moment of 4.0 μ_B for each surface Fe atom. From the Bader charge analysis, we find that the charge of the Fe_1 atoms decreases monotonically with increasing sulfur composition, from +1.1 e for Surf(−1) to +0.97 e for Surf(0) and +0.93 e for Surf(+1). This indicates a partial oxidation of Fe_1 atoms ($Fe^{2+} \rightarrow Fe^{3+}$) to compensate for the effects of surface termination and structural relaxation. In particular, the S_{1b} atoms of Surf(−1) convert to S^{2-}, as suggested by their Bader charge of −1.02 e, which is more than twice that of bulklike S (−0.43 e). Therefore, we conclude that S-deficient Surf(n) undergo a partial charge transfer of the type $Fe^{2+} + S^{1-} \rightarrow Fe^{3+} + S^{2-}$ and that the charge redistribution

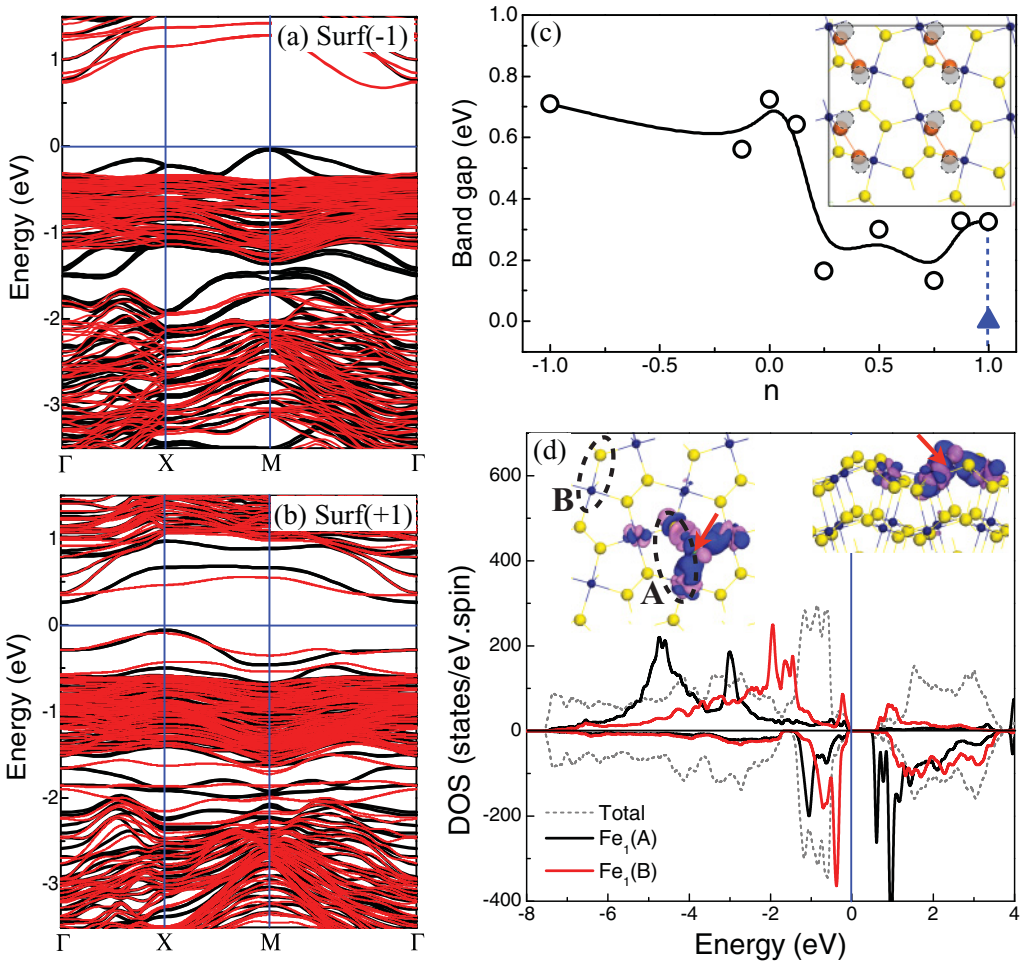

FIG. 4. (Color online) Band structure of (a) Surf(−1) and (b) Surf(+1), with bold black and thin red (gray) lines for states in the majority and minority spin channels, respectively. (c) The band gap as a function of the surface composition parameter n. The solid triangle at $n = 1.0$ represents the band gap for Surf(+1) when sulfur dimerization is disallowed in the calculations. The inset in (c) shows the top view of the two atomic structures of Surf(+1) with orange (dark gray) and gray spheres indicating the positions of surface sulfur atoms with and without dimerization, respectively. The calculated (experimental) bulk band gap is 1.02 eV (0.95 eV). (d) The projected density of states (PDOS) for surface Fe atoms on Surf(−0.125). The positive and negative values indicate states in the majority and minority spin channels, respectively. The insets in (d) are the top and side views of charge density difference, $\rho_{\mathrm{Surf}(0)} - \rho_{\mathrm{Surf}(-0.125)} - \rho_{\mathrm{S}}$, with blue (dark gray) and purple (light gray) isosurfaces denoting electron accumulation and depletion, respectively. The position of the surface sulfur vacancy on Surf(−0.125) is indicated by the red (gray) arrow. Dashed A and B ellipses mark defected and defect-free regions on Surf(−0.125), respectively.

shifts the band-edge states by a few tenths of an eV, fortuitously maintaining a relatively large band gap.

This mechanism is also operative on other sulfur-deficient pyrite surfaces, such as Surf(−0.125). As shown in Figs. 4(c) and 4(d), Surf(−0.125) maintains a sizable band gap of 0.56 eV despite having a large sulfur vacancy density of 8.5×10^{13} cm^{-2}. We find that the formation enthalpy for a surface sulfur vacancy ($V_{S,surface}$) is only 0.42 eV under the condition $\mu_S = -3.77$ eV, in good agreement with 0.40 eV recently reported by Yu *et al.*[30] The equilibrium $V_{S,surface}$ density should thus be rather high, particularly under weakly oxidizing growth or annealing conditions. From the top and side views of the charge density difference ($\Delta\rho = \rho_{\mathrm{Surf}(0)} - \rho_{\mathrm{Surf}(-0.125)} - \rho_{\mathrm{S}}$) in the insets in Fig. 4(d), it is evident that the elimination of $V_{S,surface}$ causes electron redistribution only in the first atomic layer around the S and Fe atoms nearest to $V_{S,surface}$. Similar to Surf(−1), the Fe and S neighbors of $V_{S,surface}$ have Bader charges of +1.07 e and −0.91 e, respectively, suggesting that partial charge transfer of the type $Fe^{2+} + S^{1-} \rightarrow Fe^{3+} + S^{2-}$ also occurs locally around $V_{S,surface}$ for Surf(−0.125). The d-shell of Fe_1(A) is fully occupied in the majority spin channel, whereas only one t_{2g} state remains occupied in the minority spin channel. The d_{xy} and d_{xz} dangling bonds projecting toward $V_{S,surface}$ form narrow bands at the bottom of the CB in the minority spin channel. If charged, $V_{S,surface}$ should behave like a donor, as commonly believed in the literature.[31] As a result, each Fe_1(A) atom possesses a large magnetic moment of 4.0 μ_B. However, the disturbance of $V_{S,surface}$ on the Fe_1(B) atom ∼6 Å away is already negligible, as manifested by the DOS features and other electronic properties in Fig. 4(d).

Our results suggest that excessive surface sulfur nonstoichiometry is a likely cause of the low V_{OC} of pyrite cells. Since the maximum V_{OC} of a Schottky or *pn* junction cannot exceed the built-in voltage (V_{bi}), which itself is limited to less

than the size of the band gap,[32] a small-gap surface layer will directly reduce V_{OC} if carriers are unable to ballistically tunnel across it. Given that the surface layer of pyrite is quite thin (<1 nm), we cannot ignore the possibility that it is essentially transparent to carriers. Assuming this is *not* the case, we expect a maximum V_{OC} of $\sim 0.7\ E_g/q$ for the stoichiometric surface and $<0.3\ E_g/q$ for S-rich surfaces (E_g is the band gap of bulk pyrite). The latter value is small enough to explain the low V_{OC} of pyrite samples that have excess surface sulfur. For stoichiometric or S-poor surfaces, however, the surface gaps seem too large to restrict V_{OC} to <200 mV. Instead, the high concentration of gap states on these surfaces [$O(5 \times 10^{14}\ \mathrm{cm}^{-2})$] may result in strong interfacial band bending and thermionic-field emission currents[32] (dark currents) that degrade V_{OC}, as proposed some time ago by Bronold *et al.*[28] Ongoing work in our labs is dedicated to passivating these surface states via interfacial engineering.

IV. CONCLUSIONS

In summary, we used systematic spin-polarized density functional calculations to elucidate the effect of surface stoichiometry on the stability and electronic structure of pyrite $FeS_2(100)$ surfaces. We find that sulfur-deficient, stoichiometric, and sulfur-rich surfaces are thermodynamically stable in SO_2-rich, H_2S-rich, and S-rich conditions, respectively. The surface band gaps are in all cases smaller than the calculated bulk pyrite band gap ($E_g = 1.02$ eV) and vary from 0.56–0.72 eV for sulfur-deficient and stoichiometric surfaces to 0–0.3 eV for sulfur-rich surfaces. The surface electronic states are localized to the first three atomic layers of the crystal (~7 Å total thickness), leaving the underlying layers bulklike in their electronic structure and band gap. The stoichiometric and S-deficient $FeS_2(100)$ surfaces display a sizeable spin polarization in the topmost layer with magnetic moments of 2 μ_B and 4 μ_B per surface Fe atom, respectively. Our calculations suggest that sulfur poor conditions should be used for the fabrication of pyrite for photovoltaic and spintronic applications.

ACKNOWLEDGMENTS

We thank the NSF SOLAR Program (Award CHE-1035218) and the UCI School of Physical Sciences Center for Solar Energy for support of this work. Calculations were performed on parallel computers at NERSC and at NSF supercomputer centers.

*Corresponding author: wur@uci.edu

[1] R. Murphy and D. R. Strongin, Surf. Sci. Rep. **64**, 1 (2009).
[2] A. Ennaoui, S. Fiechter, W. Jaegermann, and H. Tributsch, J. Electrochem. Soc. **133**, 97 (1986).
[3] K. Bilker, N. Alonso-Vante, and H. Tributsch, J. Appl. Phys. **72**, 5721 (1992).
[4] V. Antonuccia, A. S. Aricò, N. Giordano, P. L. Antonucci, U. Russo, D. L. Cocke, and F. Crea, Sol. Cells **31**, 119 (1991).
[5] A. Ennaoui, S. Fiechter, Ch. Pettenkofer, N. Alonso-Vante, K. Büker, M. Bronold, Ch. Höpfner, and H. Tributsch, Sol. Energy Mater. Sol. Cells **29**, 289 (1993).
[6] M. Bronold, Y. Tomm, and W. Jaegermann, Surf. Sci. **314**, L931 (1994).
[7] P. Raybaud, G. Kresse, J. Hafner, and H. Toulhoat, J. Phys.: Condens. Matter **9**, 11085 (1997); **9**, 11107 (1997).
[8] G. U. von Oertzen, W. M. Skinner, and H. W. Nesbitt, Phys. Rev. B **72**, 235427 (2005).
[9] A. Stirling, M. Bernasconi, and M. Parrinello, Phys. Rev. B **75**, 165406 (2007).
[10] J. Muscat, A. Hung, S. Russo, and I. Yarovsky, Phys. Rev. B **65**, 054107 (2002).
[11] M. R. Philpott, I. Y. Goliney, and T. T. Lin, J. Chem. Phys. **120**, 1943 (2004).
[12] J. Hu, Y. N. Zhang, M. Law, and R. Q. Wu, Phys. Rev. B **85**, 085203 (2012).
[13] J. D. Burton and E. Y. Tsymbal, Phys. Rev. Lett. **107**, 166601 (2011).
[14] K. Sato, L. Bergqvist, J. Kudrnovský, P. H. Dederichs, O. Eriksson, I. Turek, B. Sanyal, G. Bouzerar, H. Katayama-Yoshida, V. A. Dinh, T. Fukushima, H. Kizaki, and R. Zeller, Rev. Mod. Phys. **82**, 1633 (2010).
[15] G. Kresse and J. Furthmüller, Comput. Mater. Sci. **6**, 15 (1996).
[16] P. E. Blöchl, Phys. Rev. B **50**, 17953 (1994).
[17] J. P. Perdew, K. Burke, and M. Ernzerhof, Phys. Rev. Lett. **77**, 3865 (1996).
[18] V. I. Anisimov, F. Aryasetiaswan, and A. I. Lichtenstein, J. Phys. Condens. Matter **9**, 767 (1997).
[19] S. L. Dudarev, G. A. Botton, S. Y. Savrasov, C. J. Humphreys, and A. P. Sutton, Phys. Rev. B **57**, 1505 (1998).
[20] M. Birkholz, S. Fiechter, A. Hartmann, and H. Tributsch, Phys. Rev. B **43**, 11926 (1991).
[21] I. J. Ferrer, D. M. Nevskaia, C. de las Heras, and C. Sánchez, Solid State Commun. **74**, 913 (1990).
[22] A. V. Krukau, O. A. Vydrov, A. F. Izmaylov, and G. E. Scuseria, J. Chem. Phys. **125**, 224106 (2006).
[23] K. Reuter and M. Scheffler, Phys. Rev. B **65**, 035406 (2001).
[24] K. Ellmer and C. Hopfner, Philos. Mag. A **75**, 1129 (1997).
[25] R. Sun, M. K. Y. Chan, and G. Ceder, Phys. Rev. B **83**, 235311 (2011).
[26] D. R. Alfonso, J. Phys. Chem. C **114**, 8971 (2010).
[27] J. Puthussery, S. Seefeld, N. Berry, M. Gibbs, and M. Law, J. Am. Chem. Soc. **133**, 716 (2011).
[28] M. J. Bronold, C. Pettenkofer, and W. Jaegermann, J. Appl. Phys. **76**, 5800 (1994).
[29] R. F. W. Bader, *Atoms in Molecules: a Quantum Theory* (Oxford University Press, New York, 1990).
[30] L. P. Yu, S. Lany, R. Kykyneshi, V. Jieratum, R. Ravichandran, B. Pelatt, E. Altschul, H. A. S. Platt, J. F. Wager, D. A. Keszler, and A. Zunger, Adv. Energy Mater. **1**, 748 (2011).
[31] S. Fiechter, Sol. Energy Mater. Sol. Cells **83**, 459 (2004).
[32] S. M. Sze and K. K. Ng, *Physics of Semiconductor Devices*, 3rd ed. (Wiley Interscience, Hokoben, New Jersey, 2007).